ADVANCED FUNCTIONAL MATERIALS
www.afm-journal.de

Laser-Induced Graphene Smart Textiles for Future Space Suits and Telescopes

*Dongwook Yang, Han Ku Nam, Younggeun Lee, Soongeun Kwon, Joohyung Lee, Hyosang Yoon, and Young-Jin Kim**

Novel materials with high electrical, optical, and thermal functionalities are crucial in next-generation space missions. Astronauts' well-being demands continuous health monitoring, while stray light suppression and heat dissipation are vital for space telescopes. Here, it is demonstrated that laser-induced graphene (LIG), patterned with femtosecond laser pulses, serves as a versatile material for temperature/strain sensing, stray light absorption, and heat management for smart spacesuits and telescopes. LIG exhibits a superior temperature coefficient of resistance (−0.068% $°C^{-1}$), gauge factor of 454, optical absorption (97.57%), and heat diffusivity (6.376 $mm^2 s^{-1}$) via a single platform. Furthermore, thermal-vacuum tests confirm LIG's reliability and readiness for space missions. Under vacuum conditions (≈10^{-3} Torr) and repeated temperature changes ranging from −20 to 60 °C over a period of ≈40 h, the temperature/strain sensor, and optical absorbers maintain the functionality.

1. Introduction

During space missions, astronauts confront the challenging space environment even during intravehicular activities (IVAs). To safeguard their well-being, continuous monitoring of physiological parameters throughout the mission duration is crucial.[1] In order to manage risks, astronauts' vital health signs should be continuously monitored; the key signs include body temperature, pulse rate, respiration rate, blood pressure, and electrocardiogram.[2] While existing sensors offer valuable healthcare data, their limitations, including bulky form factors restricting astronaut mobility and the need for integration of multiple sensory platforms, hinder their convenience and effectiveness in daily IVA routines in space.[3–5] When developing a smart spacesuit for space, one should also recognize the unique conditions of space missions that require low energy consumption, tolerance to cosmic rays, antibacterial properties, convenience, and comfortability.[6–8]

For space telescopes, stray light is a major concern, as it impacts significantly the sensitivity of measurements.[9] Stray light refers to any unwanted light entering the imaging system from unintended sources, such as reflections off internal surfaces, external sources outside the field of view or the infrared lights thermally radiated from the internal part of the system. This can lead to decreased signal-to-noise ratio (SNR) and compromised data quality.[10] One of the most effective methods for controlling stray light is the use of highly absorptive baffles. Baffles are generally tubes with internal vanes that act as light traps, absorbing or blocking unwanted light. Traditionally, baffles have been made from metals with black coating with high absorptivity so as to further suppress the stray light.[11–16] These coatings should be over a broad wavelength range in order to minimize as much stray light at any wavelength as possible.[17] However, traditional material coating has provided limited performances, such as weak optical absorption at infrared wavelengths, high incidence-angle dependence of the absorption coefficient, and easy delamination/peel-off effect.[18,19]

The unique properties of laser-induced graphene (LIG) could offer compelling advantages for both smart spacesuits and stray light suppression material for space telescope baffles in the harsh environment of outer space. Their exceptional electrical and thermal conductivity could enable flexible, lightweight, wearable sensors, heaters, and coolers for astronaut health monitoring and control.[20] Simultaneously, LIG's broadband optical absorptivity, thermal conductivity, and radiation shielding capability could enhance the sensitivity and longevity of space telescopes. Notably, their microlevel thickness minimizes mass, which is

D. Yang, H. K. Nam, Y. Lee, Y.-J. Kim
Department of Mechanical Engineering
Korea Advanced Institute of Science and Technology (KAIST)
Daejeon 34141, South Korea
E-mail: yj.kim@kaist.ac.kr
S. Kwon
Nano-Convergence Manufacturing Systems Research Division
Korea Institute of Machinery & Materials
156, Gajeongbuk-Ro, Yuseong-Gu, Daejeon 34103, South Korea
J. Lee
Department of Mechanical System Design Engineering
Seoul National University of Science and Technology (SEOULTECH)
Seoul 01811, South Korea
H. Yoon
Department of Aerospace Engineering
Korea Advanced Institute of Science and Technology (KAIST)
Daejeon 34141, South Korea

The ORCID identification number(s) for the author(s) of this article can be found under https://doi.org/10.1002/adfm.202411257

DOI: 10.1002/adfm.202411257

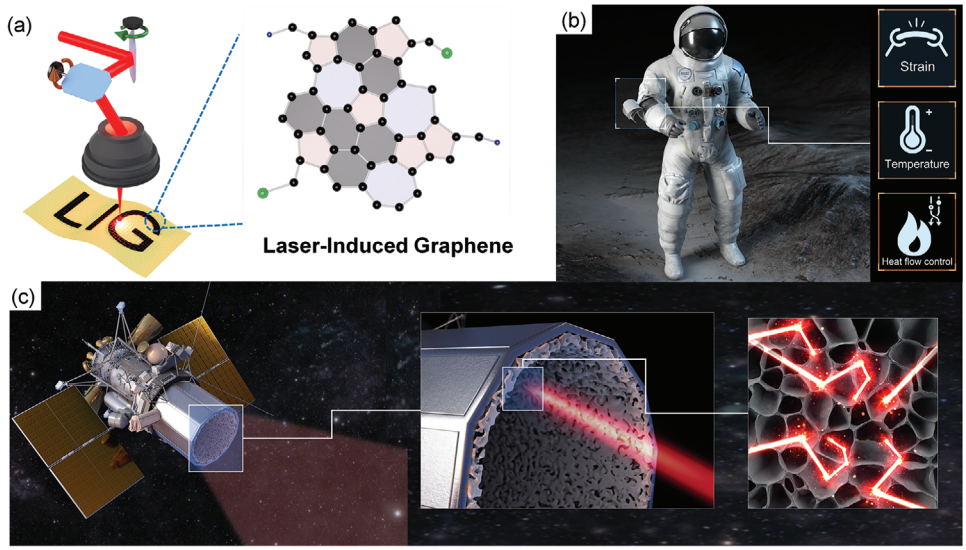

Figure 1. Schematic Illustration of the fabrication process and space applications. a) Direct laser writing of laser-induced graphene (LIG). b) LIG-based smart spacesuits support astronaut's body temperature monitoring, motion detection, and heat management. c) LIG space telescopes enable strong suppression of stray light, structural temperature sensing, and conductive heat control.

crucial for optimizing spacecraft payloads and maneuverability.[21] Thus, LIG textiles could present a synergistic opportunity to revolutionize both human exploration and astronomical understanding of the universe through their multifunctional and adaptable nature.[22–26] For real space applications, however, space compatibility tests for IVA routines in space are prerequisites, which include vibration, thermal-vacuum, and space radiation tests.[27–29] Graphene has demonstrated resilience to cosmic radiation, showing robustness when exposed to various energetic forms, such as atomic oxygen, ultraviolet light, electron beams, focused ion beam irradiation, gamma rays, and proton irradiation.[30–33] This resilience extends even to reduced graphene oxide,[34,35] carbon nanotubes,[36,37] and Kevlar textile.[38–42] There was a minor increase in the D peak but the other peaks and lattice structure were confirmed to be well maintained, which proves the strong radiation resistance of graphene.[43] Vibrational stability could be well secured by dielectric coating, which strongly adheres LIGs to the substrate materials via percolation.[44] Thermal-vacuum test is the remaining key step for LIG's real outer space applications; however, there have not been any demonstrations to date.

This paper demonstrates the ultrafast-laser-patterned LIG to realize innovative smart textile on a single integrated platform for capturing astronauts' vital signs via LIG's high electrical conductivity and to provide the best SNR to space telescopes by high-level suppression of stray lights at LIG while minimizing the unwanted internal thermal IR radiations through LIG's high thermal conductivity. By combining these key advantages of LIGs in space, astronauts and space telescopes could collect and provide more accurate and reliable data, ultimately enabling astronomers to make groundbreaking discoveries about the universe and opening new markets through new space programs.

2. Results and Discussions

2.1. Direct Writing of LIG Textiles for Outer Space Applications

Figure 1a illustrates our direct-laser-writing system, consisting of a Yb-doped fiber femtosecond laser, beam-delivery optics, power/polarization control units, and a Galvano scanner. The laser emits a repetitive pulse train of 200 kHz at a center wavelength of 1040 nm with a pulse duration of 255 fs. The laser's maximum average power is 7.0 W and the beam-scanning speed can be set from 0 to 1000 mm s^{-1} for the optimal LIG fabrication. The combination of a Galvano scanner and f-theta lens directs and focuses the laser beam onto the target sample with a spot diameter of 70 µm along preprogrammed arbitrary patterns.

LIGs on textiles exhibit significant promise for diverse applications in outer space environments owing to their distinctive properties and manufacturing advantages.[45] In the context of space telescope systems, the 3D porosity of LIG, known for enhancing light absorption, renders it a compelling candidate for telescope baffles. Baffles, crucial in preventing stray light interference, could benefit from LIG's porous structure, ultimately improving imaging capabilities.[46–50] Furthermore, LIG's remarkable sensitivity as a strain sensor, attributed to crack propagation and the tunneling effect, positions it as a valuable tool for structural health monitoring of astronauts, spacecraft, and space telescopes, offering real-time insights into mechanical stress and deformation.[32–51] The high-temperature coefficient of resistance (TCR) of LIG also positions it as a suitable material for crafting high-sensitivity temperature sensors, ensuring precise temperature measurements in outer space.[56] Additionally, the exceptional heat conductivity of LIG can contribute to efficient heat flow control, which is vital for thermal management in space applications where thermal convection does not work.[57] The simple production and cost-effectiveness of LIG make it highly

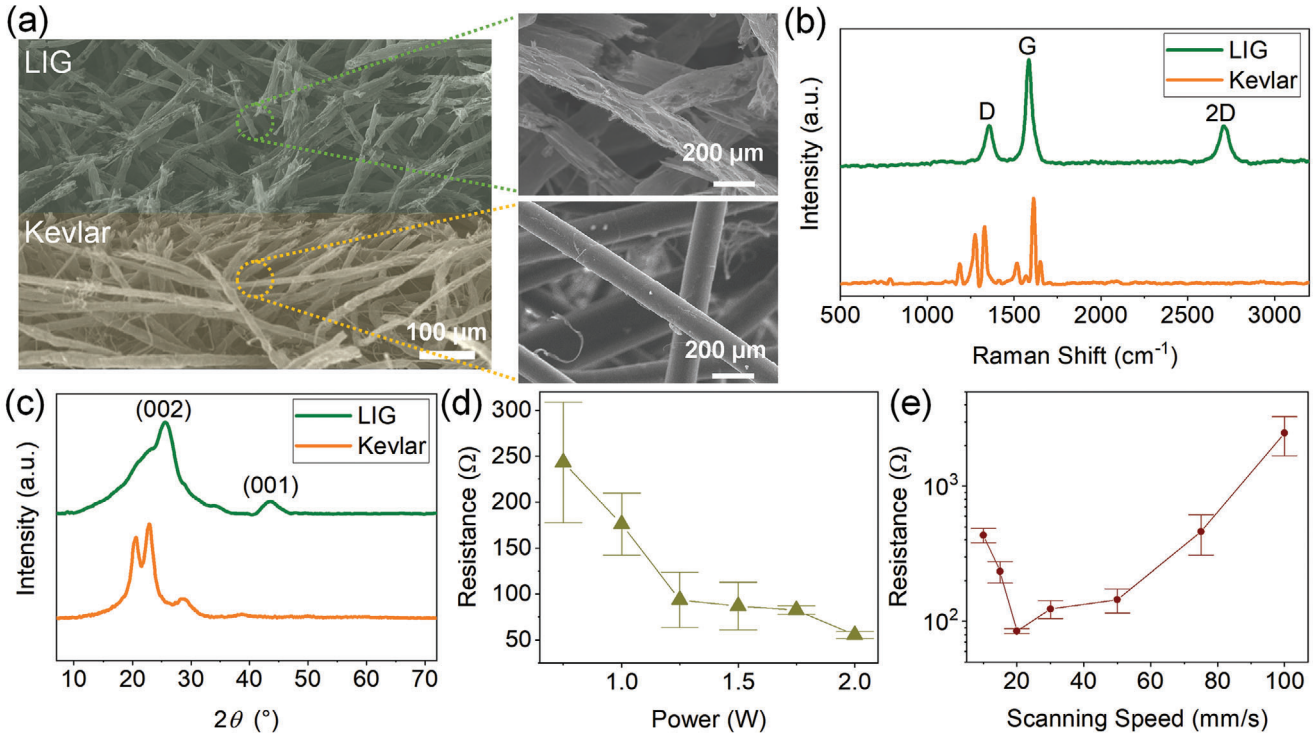

Figure 2. Characterization of LIG. a) SEM image displaying the intersection of LIG and pristine Kevlar. b) Raman spectrum of LIG and Kevlar. c) XRD pattern of LIG and pristine Kevlar. d) Resistance changes with laser power from 0.5 to 2.0 W. e) Resistance changes with different scanning speeds from 10 to 100 mm s^{-1}.

appealing for use in outer space missions. While the potential applications are promising, it is imperative to address challenges associated with the space environment, such as extreme temperatures, vacuum conditions, and radiation exposure.

2.2. Characterization of LIG and Kevlar

In **Figure 2a**, scanning-electron microscope (SEM) images depict the surface morphologies of the original Kevlar textile and the LIG directly converted by NIR femtosecond laser, utilizing an average power of 1.5 W and a scanning speed of 20 mm s^{-1}. The pristine Kevlar textile exhibits a fine surface under higher magnification, while the femtosecond-laser-patterned LIG displays a 3D porous structure. The porous structure of LIG contributes the high optical absorption due to the multireflections inside the hollow fiber. Figure 2b,c exhibits the chemical characterization of Kevlar textile and LIG via Raman spectroscopy and X-ray diffraction, respectively. Raman spectroscopy is an invaluable tool for characterizing 2D carbon materials. Employing a 500 nm excitation laser-focused on the samples through a 50× objective lens, Raman peaks were observed using a notch filter. In Figure 2b, the spiky peaks are investigated in the Raman spectrum of Kevlar, and the Raman spectrum of LIG reveals three prominent peaks at 1357, 1585, and 2709 cm^{-1}, corresponding to the D, G, and 2D peaks, respectively. The D peak indicates the defects or disorders within the graphene lattice, providing graphene's structural integrity. The G peak aligns with the E2g phonon at the Brillouin zone center, serving as an identifier for the presence of sp2 hybridized carbon atoms arranged in a hexagonal lattice. The 2D peak is employed for assessing the number of graphene layers and the overall quality of graphene.[58] The I_D/I_G ratio, indicating the defect density of the LIG, is measured at 0.339. The 2D peak's width was low at 68 cm^{-1} in full-width-half-maximum which represents good graphene quality. Figure 2c shows the XRD pattern of Kevlar and LIG. With the pristine Kevlar, three discernible peaks are at $2\theta = 20.7°$, 22.9°, and 28.7°, corresponding to the (110), (200), and (004) planes, respectively.[60] In contrast, the LIG exhibits two pronounced peaks at $2\theta = 25.9°$ and 43.4°, aligning with the (002) and (100) planes. This observation confirms the formation of graphitized structures characterized by a 0.3–0.4 nm interlayer spacing.[61,62] To employ LIG as a resistive-type strain sensor and temperature sensor, the electrical conductivity of the LIG was optimized with different laser power and scanning speed, as depicted in Figure 2d,e. Figure 2d shows the electrical resistance across the laser average power from 0.5 to 2.0 W while keeping the scanning speed at 15 mm s^{-1}. Simultaneously, Figure 2d displays electrical resistances varying the scanning from 10 to 100 mm s^{-1}, while maintaining an average power of 1.5 W. Typically, an increase in heat influx (achieved through higher power and lower scanning speed) leads to elevated electrical conductivity due to the formation of 5,6,7 membered carbon ring with high conductivity.[45,63–65] However, exceeding a certain threshold of heat influx results in decreased electrical conductivity due to the ablation of LIG, as illustrated in Figure 2e. Also, the standard deviation is attributed to the textile's inherent structural variability and the inhomogeneity of LIG resulting from the laser patterning strategy.[55,66,67]

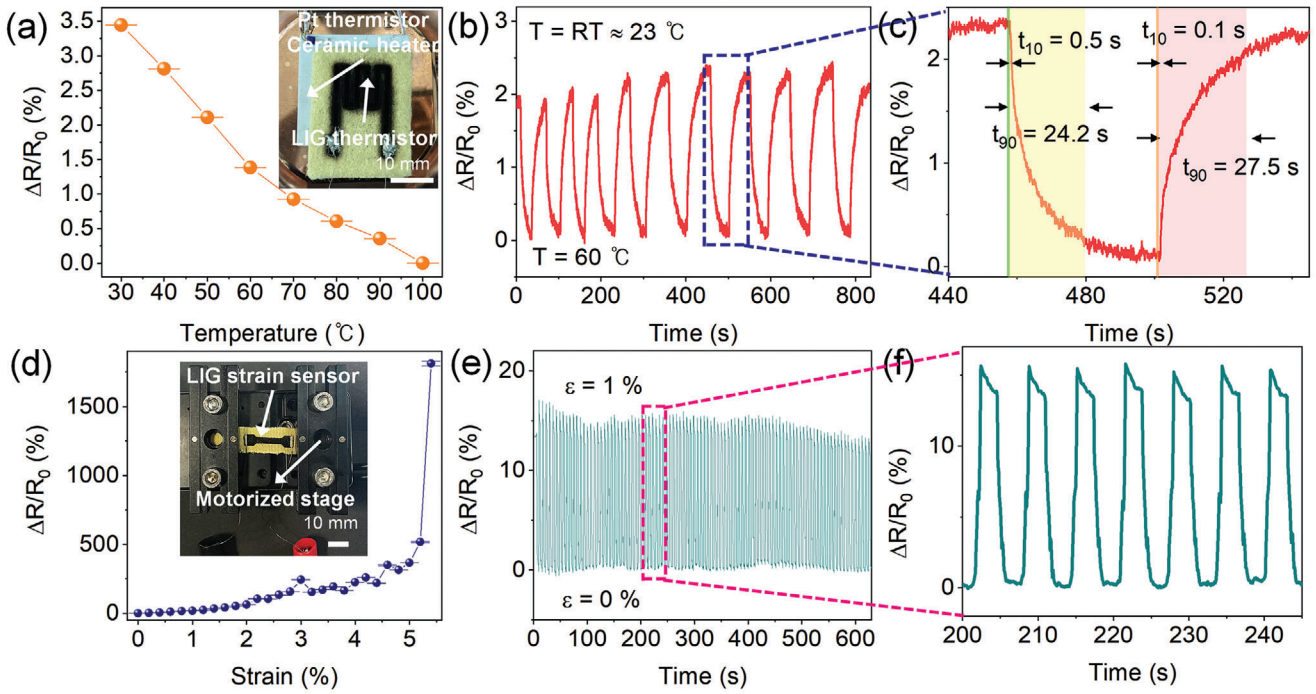

Figure 3. LIG-based temperature sensor and strain sensor. a) LIG temperature sensor's temperature–resistance relationship. b,c) Time response of a LIG temperature sensor. d) LIG stain sensor's strain-resistance change relationship. e,f) Time response and reliability test results of a LIG strain sensor under 1.0% strain over 100 cycles.

2.3. LIG Textiles for Wearable Astronaut Electronics

For monitoring astronauts' body temperature in outer space, a temperature sensor was created on the Kevlar textile by ultrafast femtosecond laser irradiation with an average power of 1.5 W and scanning speed of 50 mm s^{-1}, as shown in **Figure** 3a–c. The temperature–resistance curve is obtained by incrementally raising the temperature from 30 to 100 °C, while recording the average electrical resistance at each temperature interval, demonstrating a negative temperature coefficient of resistance (TCR) of −0.068% $°C^{-1}$ (30–60 °C), as depicted in Figure 3a. This TCR demonstrates excellent quality compared with previous articles, such as PI-LIG transferred to cotton textile (−0.05% $°C^{-1}$)[22] and graphene synthesized by chemical vapor deposition (CVD) process (−0.0017% $°C^{-1}$).[68] Figure 3b shows repetitive test results via stepwise temperature control between 23 and 60 °C. The recorded response and recovery times were 24.2 and 27.5 s for approaching 90% of the final value, which were 0.5 and 0.1 s for 10% settling, respectively. The thermal response observed can be attributed to factors, such as the 3 mm thickness of the Kevlar, the spacing between the Kevlar and the ceramic heater, and Kevlar's thermal conductivity of 0.04 W mK^{-1}. The negative TCR observed in LIG based temperature sensors can be attributed to the unique properties of graphene. Unlike most metals, which exhibit a positive TCR due to increased phonon scattering, graphene shows a negative TCR where resistance decreases as temperature rises. This behavior is due to the semimetallic nature of graphene, where increased temperature enhances the mobility of charge carriers (electrons and holes), reducing resistance. Key mechanisms contributing to this include thermally activated hopping, which increases active charge carriers, shifts in graphene's band structure, and the complex interactions of phonon scattering.[69–73] These results demonstrate that our LIG temperature sensor on Kevlar shows excellent performance for embedding in spacesuits.

The LIG-based strain sensor is fabricated directly onto the Kevlar textile to track astronauts' local body motions. To achieve higher patterning resolution and expand the measurable strain range, a 15% prestrain was applied to the Kevlar textile using a motorized stage. Subsequently, LIG was patterned according to a predesigned rectangular shape (5 × 15 mm^2) with an average power of 1.5 W and a scanning speed of 25 mm s^{-1}. As shown in Figure 3d, the strain was gradually increased from 0% to 5.4%. The gauge factor (GF), indicating the sensitivity of the strain sensor, was evaluated as 30 (from 0% to 2%) and 454 (from 4.8% to 5.4%), respectively. This variation in GF is attributed to crack propagation, tunneling effect, and contact resistance.[67] The crack propagation and the tunneling effect play pivotal roles in enhancing the GF. Conversely, the application of strain can lead to a reduction in contact resistance, resulting in a minor decrease of resistance as shown in the strain range of 3.2%–4.8%. Our strain sensor's GF is better than previous reports, such as the graphene on textile by thermal reduction (26),[74] LIG on PI textile (27),[75] PI-LIG transferred to cotton textile (114).[22] The durability of the strain sensor was evaluated under a 1% strain for 100 cycles, as shown in Figure 3e,f. The response times of the strain sensor can be analyzed under the strains from 0% to 1.0%, as shown in Figure 3f. A rapid strain change of 1% at a speed of 0.15 mm s^{-1} was recorded with a time scale of 0.1 s. In extended cyclic test up to 1200 cycles, the minor fluctuations

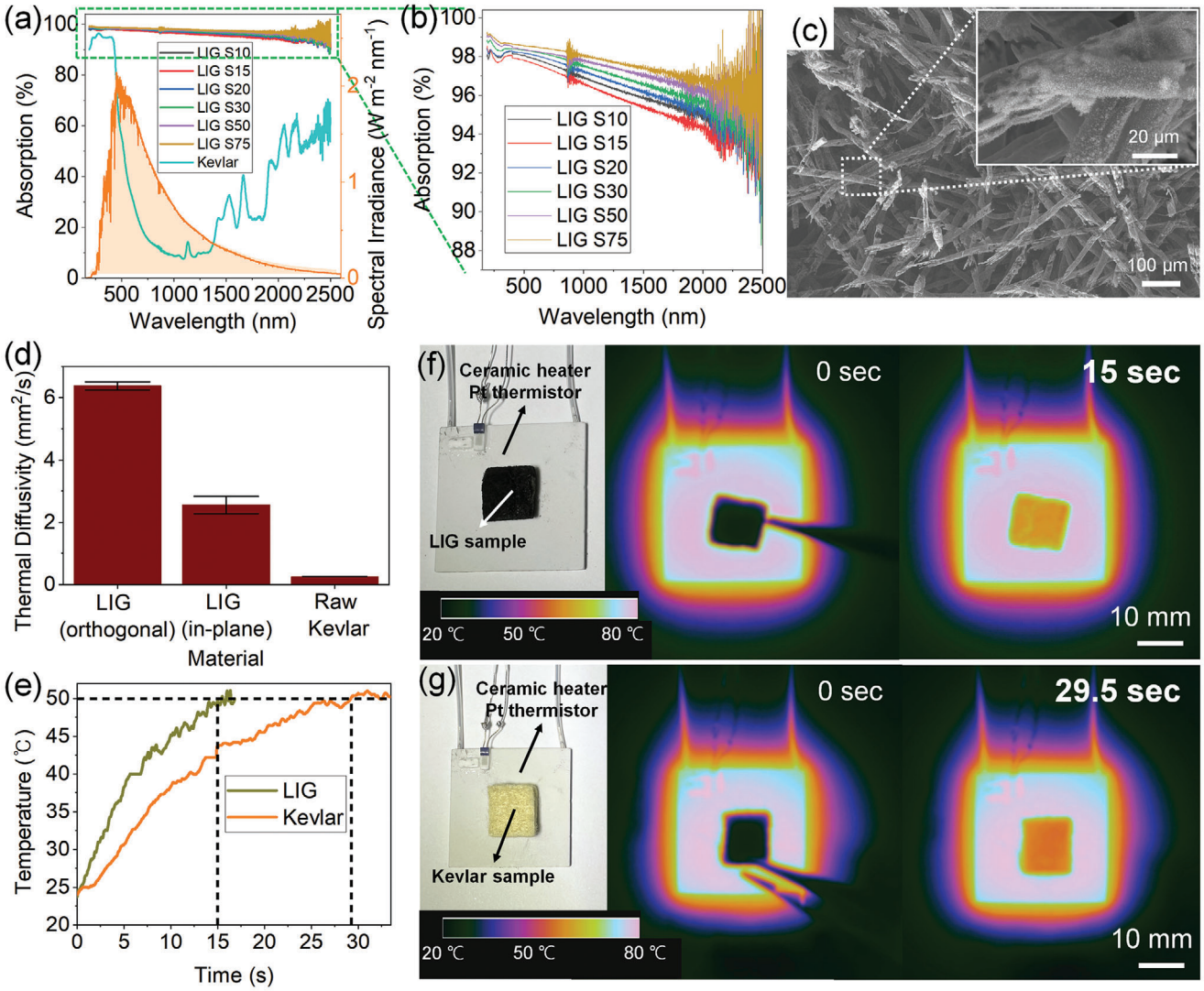

Figure 4. Light absorption and thermal diffusivity of LIG. a,b) Light absorption of LIG and raw Kevlar. c) SEM images of LIG S75. d) Thermal diffusivity of LIG and Kevlar. e–g) Heat diffusion demonstration of LIG and raw Kevlar in-depth direction.

observed are attributed to overshoot of stage control. However, in magnified figure, it shows the reliability and durability of the strain sensor (Figure S2, Supporting Information). The flexibility of LIG/Kevlar textile was validated through strain tests up to 5.4% and over 1200 cycles of repeated strain at 1%, demonstrating minimal resistance changes and confirming the material's high durability. These results underscore the robustness and suitability of LIG/Kevlar textiles for flexible aerospace applications.

2.4. LIGs for Higher SNR, Thermally Stable, and Smart Telescopes

Figure 4 presents the optical absorption spectrum and thermal properties of double-sided LIG, single-sided LIG, and Kevlar for higher SNR space telescopes. The absorption values are attained by subtracting transmittance and reflectance from the total incident power in the wavelength range from 190 to 2500 nm. In Figure 4a, ASTM E-490 AM0, the standard solar spectrum is shown, where we can check that 99% of solar energy falls between 280 and 2500 nm. The samples, denoted as LIG S10 to LIG S75, are fabricated using femtosecond laser patterning with an average laser power of 1.5 W with scanning speeds from 10 to 75 mm s^{-1}. The absorption integrated over ≈190–2500 nm for LIG S10, LIG S15, LIG S20, LIG S30, LIG S50, LIG S75, and raw Kevlar is 96.23%, 95.77%, 96.45%, 96.81%, 97.23%, 97.57%, and 37.95%, respectively. This confirms that laser patterning can increase the optical absorption from 37.95% to 96.81% by 58.86% or by 2.55 times. This high-level absorption is enabled due to the forest-like porous fiber structure in Figure 4c[76] (Figure S1, Supporting Information). This optical absorption of LIG is comparable with previous reports, such as LIG from PI (99%)[76] and nickel nanoparticle on LIG from Kevlar (97%).[66]

The absorbed optical power can be converted into local heat and cause unexpected local structural distortion of the telescope or even make secondary infrared optical radiation that can reach

the photodetector and deteriorate the SNR. This issue can be also resolved by using LIG as a thermal conductor for heat dissipation. Therefore, we measured the thermal diffusivity of raw Kevlar and LIG (LIG S20, double-sided patterning) in thickness and perpendicular directions by using a laser flash analyzer (LFA), as shown in Figure 4d. The raw Kevlar yields a thermal diffusivity of 0.258 $mm^2\ s^{-1}$, while that of LIG in the thickness and in-plane directions are measured at 6.376 and 2.554 $mm^2\ s^{-1}$, respectively (Raw data are shown in Figures S3, S4, and S5, Supporting Information). The thermal diffusivity shows excellent value compared to the previous research (LIG from PI, 1.6 $mm^2\ s^{-1}$).[77] Subsequently, a heat conduction demonstration experiment was performed by placing both Kevlar and LIG samples on a ceramic heater set at 80 °C, as illustrated in Figure 4e–g. The time taken to reach the high-temperature state of 50 °C was dramatically shortened from 29.5 to 15.0 s by 50%. Also, we estimated emissivity of LIG to be between 0.7 and 0.95, based on similar carbon-based materials, such as multilayered graphene,[78,79] carbon nanotube (CNT),[80] and reduced graphene oxide.[81,82] Applying Kirchhoff's law and considering the high solar absorptance, we infer that LIG/Kevlar textile likely has an emissivity near 0.95–0.97, making it well-suited for applications requiring effective thermal regulation.[83–85] Furthermore, differential scanning calorimetry (DSC) measurements conducted from −30 to 65 °C on Kevlar and LIG samples to calculate the thermal conductivity[86] (Figure S6, Supporting Information). The specific heat capacity values at room temperature (25 °C) were found to be 1.6549 J gK^{-1} for Kevlar and 2.0245 J gK^{-1} for LIG. Using these values, the thermal conductivity of LIG was determined to be 18.6 W $m^{-1}\ K^{-1}$, which is significantly higher than reported results, such as LIG from Polyimide (PI) (0.85 W $m^{-1}\ K^{-1}$),[87] LIG from PI with P3HT (1.72 W $m^{-1}\ K^{-1}$),[88] and multilayer LIG from PI (13.05 W $m^{-1}\ K^{-1}$).[89] This increased thermal conductivity highlights the potential of LIG/Kevlar textile for effective heat dissipation in applications requiring robust thermal management, particularly in space environments.

2.5. Thermal-Vacuum Test of LIGs for Space Qualification

To prove the LIG's readiness for spacesuits and telescopes, the thermal-vacuum tests were performed for the LIG-based temperature sensor, strain sensor, and light absorption coatings, as shown in **Figure 5a**. Under a vacuum level of ≈10^{-3} Torr, the temperature of the LIG devices was controlled from −20 to 60 °C; the two operation cycles had the dwell time of 2 h, while the eight survival cycles had the same temperature profile with the dwell time of 1 h. This temperature and vacuum level correspond to the IVA conditions in space.[90–93] The electrical signals from the temperature and strain sensors were continuously monitored for the whole test cycle (operation and survival cycles) using a source measurement unit (SMU) with a time scale of 30 s, as shown in Figure 5b. The temperature sensor detected the temperature variations from −20 to 60 °C well even under vacuum conditions. The strain sensor also responded to temperature changes because of the thermal expansion of the 3D-printed polylactic acid (PLA) base plate's thermal expansion (with 68 μm $m^{-1}\ K^{-1}$) during the operational tests. In real applications, the strain information can be extracted without temperature dependence by orthogonalization of two signals with the aid of the temperature sensor installed nearby. Following the thermal vacuum test, the final performance of the temperature sensor, strain sensor, and optical absorber was re-evaluated to validate their durability in extreme space conditions. Figure 5c shows the temperature measurement results over 10 repetitive cycles between 25 and 60 °C, revealing only negligible changes in resistance; the response and relaxation times also show slight decreases of less than 3.48% from 24.4 and 28.7 s to 24.2 and 27.5 s, respectively. The strain sensor was also reassessed under a 1.0% strain for 100 cycles, as shown in Figure 5d, which showed negligible decreases as well. Finally, the optical absorption of the LIG S75 sample was re-evaluated after the thermal-vacuum tests, as shown in Figure 5e. LIG S75 shows an optical absorption of 97.7% across the wavelength range from 190 to 2500 nm, which is a slightly better value than before. These series of results confirm that LIG-based sensors, optical absorbers, and heat management devices can be readily used for next-generation spacesuits and space telescopes in extreme space conditions.

3. Conclusion

In conclusion, this paper proposes a novel approach for the simple and cost-effective production of LIG textiles, showcasing their versatile applicability in future space applications, especially wearable spacesuits and smart space telescopes. LIG's unique performances, including high electrical/thermal conductivity and high optical absorption, were confirmed by a series of experiments. The resulting LIG smart textiles exhibit outstanding performance in monitoring astronauts' vital signals as well as suppressing undesirable stray lights and dissipating the heat in telescopes. Moreover, the thermal-vacuum tests assessed the environmental durability of LIG-based sensors and optical absorbers under space conditions. These series of results are expected to accelerate the widespread utilization of LIGs in future space missions.

4. Experimental Section

Direct Laser Writing of LIG on Kevlar: The experiments utilized a femtosecond laser setup comprised of a Yb-doped fiber femtosecond laser (LASERNICS, FUPL-250-6), along with beam steering optics (Thorlabs, Inc.), an f-theta lens for precise IR beam focusing (Wavelength Optoelectronics), and a Galvano scanner system (Han's Laser, PSXA104A) by a computerized control system (Figure S7, Supporting Information). The laser emitted pulses of 255 fs at a wavelength of 1035.67 nm and operated at a repetition rate of 201.5 kHz (Figures S8 and S9, Supporting Information). The beam was angularly scanned and focused onto a substrate, achieving a spot size of 70.95 μm (Figure S10, Supporting Information). These procedures were conducted in standard lab conditions with a temperature of 25 °C and a relative humidity of 25%.

Characterization of Kevlar and LIG: Morphological characterization was conducted using a Hitachi SEM (SU5000) with a platinum coating on samples. The Raman spectroscopic analysis was carried out with a HORIBA LabRAM HR Revolution spectrometer using a 500 nm laser and a 50x objective lens. XRD patterns were acquired with a Rigaku SmartLab using Cu Kα radiation. Optical absorption was assessed with a UV–VIS/NIR Spectrophotometer (Lambda 1050, Perkin Elmer) across a spectrum of 190–2500 nm. Thermal diffusivity measurements were obtained using a laser flash apparatus (LFA 467, NETZSCH).

LIG Sensor Test: An IR femtosecond laser, operating at an average power of 1.5 W and a scanning speed of 50 mm s^{-1}, was employed to

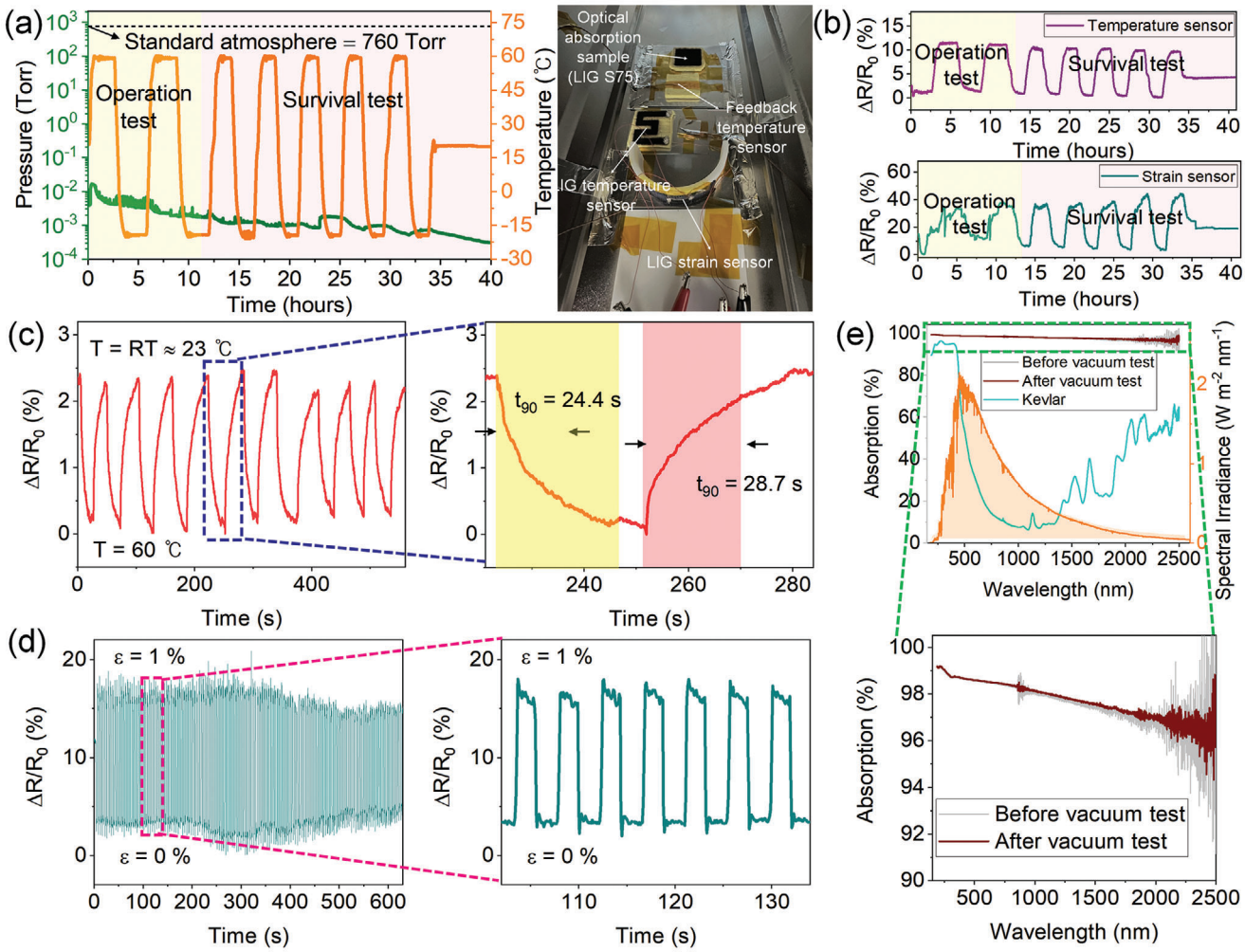

Figure 5. Thermal-vacuum test and performance retention after the test. a) Environmental conditions of repetitive thermal-vacuum tests. b) Real-time resistance changes of LIG-based temperature and strain sensors during the thermal-vacuum tests. c–e) After the thermal-vacuum tests, the LIG temperature sensor, strain sensor, and light absorbers were reassured.

pattern the temperature sensor. The temperature tests were conducted using a metal ceramic heater (Thorlabs, HT24S2) with dimension of 28 mm × 28 mm and power of 24 W, integrating a platinum resistance temperature detector (Thorlabs, TH100PT) for monitoring the temperature. The heater was equipped with an integrated thermocouple, providing temperature control with an accuracy of ±1 °C. Additionally, a prestretched knit Kevlar was processed into a rectangular shape (5 × 15 mm) using an IR femtosecond laser set to the same power and a reduced scanning speed of 25 mm s^{-1}. The strain was applied using a motorized stage (Thorlabs, DDSM100/M) and measured with a Source Measure Unit (Keysight, B2912A).

Supporting Information

Supporting Information is available from the Wiley Online Library or from the author.

Acknowledgements

Korean National Research Foundation (Nos. NRF-2020R1A2C210233813, NRF-RS-2024-00401786 Ministry of Agriculture, Food and Rural Affairs (No. MAFRA: RS-2024-00401642) R&D Program for Forest Science Technology (Project No. 2023488B10-2325-AA01) provided by Korea Forest Service (Korea Forestry Promotion Institute).

Conflict of Interest

The authors declare no conflict of interest.

Data Availability Statement

The data that support the findings of this study are available from the corresponding author upon reasonable request.

Keywords

direct laser writing, laser-induced graphene, smart textile, space-qualified

Received: June 27, 2024
Revised: August 27, 2024
Published online:

[1] E. Y. W. Chang, *Acta Astronaut.* **2021**, *178*, 117.
[2] P. Weiss, M. P. Mohamed, T. Gobert, Y. Chouard, N. Singh, T. Chalal, S. Schmied, M. Schweins, T. Stegmaier, G. T. Gresser, G. Groemer, N. Sejkora, S. Das, R. Rampini, M. Hołyńska, *Adv. Mater. Technol.* **2020**, *5*, 2000028.
[3] E. E. Sigaleva, O. B. Pasekova, N. V. Degterenkova, L. Y. Marchenko, E. I. Matsnev, *Hum. Physiol.* **2023**, *49*, 649.
[4] F. Braunschweig, *Eur. J. Intern. Med.* **2023**, *115*, 39.
[5] H. L. Paul, K. R. Diller, *J. Biomech. Eng.* **2003**, *125*, 639.
[6] I. Levchenko, K. Bazaka, T. Belmonte, M. Keidar, S. Xu, *Adv. Mater.* **2018**, *30*, 1802201.
[7] K. P. Sibin, A. C. Mary Esther, H. D. Shashikala, A. Dey, N. Sridhara, A. K. Sharma, H. C. Barshilia, *Sol. Energy Mater. Sol. Cells* **2018**, *176*, 134.
[8] A. Carmel Mary Esther, N. Sridhara, S. V. Sebastian, P. Bera, C. Anandan, D. Rangappa, A. Kumar Sharma, A. Dey, *Ceram. Int.* **2016**, *42*, 2589.
[9] V. Y. Terebizh, *Exp. Astron.* **2001**, *11*, 171.
[10] J. J. Bock, A. E. Lange, H. Matsuhara, T. Matsumoto, T. Onaka, S. Sato, *Appl. Opt.* **1995**, *34*, 2268.
[11] A. K. Sharma, H. Bhojraj, V. K. Kaila, H. Narayanamurthy, *Met. Finish.* **1997**, *95*, 14.
[12] Y. Goueffon, L. Arurault, C. Mabru, C. Tonon, P. Guigue, *J. Mater. Process. Technol.* **2009**, *209*, 5145.
[13] M. J. Persky, *Rev. Sci. Instrum.* **1999**, *70*, 2193.
[14] R. Ghosh, A. Dey, M. K. Kavitha, H. K. Thota, R. U. Rani, A. Rajendra, K. Das, *Ceram. Int.* **2022**, *48*, 35689.
[15] D. Madhuri, R. Ghosh, M. A. Hasan, A. Dey, A. M. Pillai, K. S. Anantharaju, A. Rajendra, *J. Mater. Eng. Perform.* **2021**, *30*, 4072.
[16] D. Madhuri, R. Ghosh, M. A. Hasan, A. Dey, A. M. Pillai, M. Angamuthu, K. S. Anantharaju, A. Rajendra, *Ceram. Int.* **2022**, *48*, 35906.
[17] M. Senthil Kumar, C. S. Narayanamurthy, A. S. Kiran Kumar, *J. Opt.* **2016**, *45*, 180.
[18] V. Villalba, H. Kuiper, E. Gill, *Journal of Astronomical Telescopes Instruments, and Systems.* **2020**, *6*, 010902.
[19] R. K. Banyal, B. Ravindra, S. Chatterjee, *Opt. Express* **2013**, *21*, 7065.
[20] T. S. D. Le, H. P. Phan, S. Kwon, S. Park, Y. Jung, J. Min, B. J. Chun, H. Yoon, S. H. Ko, S. W. Kim, Y. J. Kim, *Adv. Funct. Mater.* **2022**, *32*, 2205158.
[21] R. Ye, D. K. James, J. M. Tour, *Adv. Mater.* **2019**, *31*, 1803621.
[22] H. Qin, A. Hajiaghajani, A. R. Escobar, A. H. A. Zargari, A. Jimenez, F. Kurdahi, P. Tseng, *ACS Appl. Nano Mater.* **2023**, *6*, 19158.
[23] T. Raza, M. K. Tufail, A. Ali, A. Boakye, X. Qi, Y. Ma, A. Ali, L. Qu, M. Tian, *ACS Appl. Mater. Interfaces* **2022**, *14*, 54170.
[24] F. Tehrani, M. Beltrán-Gastélum, K. Sheth, A. Karajic, L. Yin, R. Kumar, F. Soto, J. Kim, J. Wang, S. Barton, M. Mueller, J. Wang, *Adv. Mater. Technol.* **2019**, *4*, 1900162.
[25] W. Liu, Y. Huang, Y. Peng, M. Walczak, D. Wang, Q. Chen, Z. Liu, L. Li, *ACS Appl. Nano Mater.* **2020**, *3*, 283.
[26] I. Naseri, M. Ziaee, Z. N. Nilsson, D. R. Lustig, M. Yourdkhani, *ACS Omega* **2022**, *7*, 3746.
[27] J. Lee, K. Lee, Y. S. Jang, H. Jang, S. Han, S. H. Lee, K. I. Kang, C. W. Lim, Y. J. Kim, S. W. Kim, *Sci. Rep.* **2014**, *4*, 5134.
[28] S. Tachikawa, H. Nagano, A. Ohnishi, Y. Nagasaka, *International Journal of Thermophysics.* **2022**, *43*, 91.
[29] T. Southern, N. Moiseev, *49th Intional Conference on Environmental Systems* **2019**, *25*, 1.
[30] E. H. Åhlgren, J. Kotakoski, O. Lehtinen, A. V. Krasheninnikov, *Appl. Phys. Lett.* **2012**, *100*, 233108.
[31] M. Loeblein, A. Bolker, S. H. Tsang, N. Atar, C. Uzan-Saguy, R. Verker, I. Gouzman, E. Grossman, E. H. T. Teo, *Small* **2015**, *11*, 6425.
[32] X. Liu, J. Pu, L. Wang, Q. Xue, *J. Mater. Chem. A* **2013**, *1*, 3797.
[33] Y. He, Z. Wang, Y. Zhang, *Acta Astronaut.* **2021**, *186*, 259.
[34] E. A. Ryan, Z. D. Seibers, J. R. Reynolds, M. L. Shofner, *ACS Appl. Polym. Mater.* **2023**, *5*, 5092.
[35] Z. Seibers, M. Orr, G. S. Collier, A. Henriquez, M. Gabel, M. L. Shofner, V. L. Saponara, J. Reynolds, *Polym. Eng. Sci.* **2020**, *60*, 86.
[36] B. Earp, J. Hubbard, A. Tracy, D. Sakoda, C. Luhrs, *Composites, Part B* **2021**, *219*, 108874.
[37] N. Atar, E. Grossman, I. Gouzman, A. Bolker, V. J. Murray, B. C. Marshall, M. Qian, T. K. Minton, Y. Hanein, *ACS Appl. Mater. Interfaces* **2015**, *7*, 12047.
[38] J. E. Miller, R. J. McCandless Jacobs, B. D. Jacobs, *NASA Technical Reports Server (NTRS)* **2021**, 20210020869.
[39] M. Pugliese, V. Bengin, M. Casolino, V. Roca, A. Zanini, M. Durante, *Radiat. Environ. Biophys.* **2010**, *49*, 359.
[40] J. Ma, Q. Wei, H. Fan, Z. Qi, N. Hu, *Coatings* **2022**, *12*, 584.
[41] L. Narici, M. Casolino, L. Di Fino, M. Larosa, P. Picozza, A. Rizzo, V. Zaconte, *Sci. Rep.* **2017**, *7*, 1.
[42] P. Priyanka, A. Dixit, H. S. Mali, *Iran. Polym. J.* **2019**, *28*, 621.
[43] S. Kumar, A. Tripathi, S. A. Khan, C. Pannu, D. K. Avasthi, *Appl. Phys. Lett.* **2014**, *105*, 133107.
[44] H. Huang, X. Tang, F. Chen, J. Liu, D. Chen, *J. Nucl. Mater.* **2017**, *493*, 322.
[45] D. Yang, H. K. Nam, T. S. D. Le, J. Yeo, Y. Lee, Y. R. Kim, S. W. Kim, H. J. Choi, H. C. Shim, S. Ryu, S. Kwon, Y. J. Kim, *ACS Nano* **2023**, *17*, 18893.
[46] S. Y. Xia, Y. Long, Z. Huang, Y. Zi, L. Q. Tao, C. H. Li, H. Sun, J. Li, *Nano Energy* **2022**, *96*, 107099.
[47] Y. Maithani, B. R. Mehta, J. P. Singh, *New J. Chem.* **2022**, *47*, 1832.
[48] S. Kwon, T. Lee, H. J. Choi, J. Ahn, H. Lim, G. Kim, K. B. Choi, J. J. Lee, *J. Power Sources* **2021**, *481*, 228939.
[49] J. Cheng, S. Tang, Z. Lin, Z. Wang, D. Wu, D. Wang, C. Liu, Z. Cao, *Appl. Surf. Sci.* **2024**, *648*, 159073.
[50] Y. Rao, M. Yuan, B. Gao, H. Li, J. Yu, X. Chen, *J. Colloid Interface Sci.* **2023**, *630*, 586.
[51] T. S. Dinh Le, J. An, Y. Huang, Q. Vo, J. Boonruangkan, T. Tran, S. W. Kim, G. Sun, Y. J. Kim, *ACS Nano* **2019**, *13*, 13293.
[52] J. Cheng, Z. Lin, D. Wu, C. Liu, Z. Cao, *J. Hazard. Mater.* **2022**, *436*, 129150.
[53] A. Lipovka, M. Fatkullin, S. Shchadenko, I. Petrov, A. Chernova, E. Plotnikov, V. Menzelintsev, S. Li, L. Qiu, C. Cheng, R. D. Rodriguez, E. Sheremet, *ACS Appl. Mater. Interfaces* **2023**, *15*, 38946.
[54] M. Parmeggiani, S. Stassi, M. Fontana, S. Bianco, F. Catania, L. Scaltrito, A. Lamberti, *Smart Mater. Struct.* **2021**, *30*, 105007.
[55] H. Wang, H. Wang, Y. Wang, X. Su, C. Wang, M. Zhang, M. Jian, K. Xia, X. Liang, H. Lu, S. Li, Y. Zhang, *ACS Nano* **2020**, *14*, 3219.
[56] T. S. D. Le, S. Park, J. An, P. S. Lee, Y. J. Kim, *Adv. Funct. Mater.* **2019**, *29*, 1902771.
[57] M. K. Smith, D. X. Luong, T. L. Bougher, K. Kalaitzidou, J. M. Tour, B. A. Cola, *Appl. Phys. Lett.* **2016**, *109*, 253107.
[58] L. M. Malard, M. A. Pimenta, G. Dresselhaus, M. S. Dresselhaus, *Phys. Rep.* **2009**, *473*, 51.
[59] Barkoula, C. Arrieta, E. David, P. Dolez, T. Vu-Khanh, *Polymer composites* **2011**, *32*, 362.
[60] S. Sharma, A. K. Pathak, V. N. Singh, S. Teotia, S. R. Dhakate, B. P. Singh, *Carbon* **2018**, *137*, 104.
[61] S. H. Huh, *Carbon* **2014**, *78*, 617.
[62] J. Hass, R. Feng, J. E. Millán-Otoya, X. Li, M. Sprinkle, P. N. First, W. A. De Heer, E. H. Conrad, C. Berger, *Phys. Rev. B: Condens. Matter Mater. Phys.* **2007**, *75*, 214109.
[63] A. Vashisth, M. Kowalik, J. C. Gerringer, C. Ashraf, A. C. T. Van Duin, M. J. Green, *ACS Appl. Nano Mater.* **2020**, *3*, 1881.
[64] Y. Dong, S. C. Rismiller, J. Lin, *Carbon* **2016**, *104*, 47.
[65] Y. Chen, J. Long, S. Zhou, D. Shi, Y. Huang, X. Chen, J. Gao, N. Zhao, C. P. Wong, *Small Methods* **2019**, *3*, 1900208.

[66] S. Zhu, Z. Lei, Y. Dou, C. W. Lou, J. H. Lin, J. Li, *Chem. Eng. J.* **2023**, *452*, 139403.
[67] Y. J. Kim, D. Yang, H. K. Nam, T. S. D. Le, Y. Lee, S. Kwon, *CIRP Ann.* **2022**, *71*, 473.
[68] G. Rajan, J. J. Morgan, C. Murphy, E. Torres Alonso, J. Wade, A. K. Ott, S. Russo, H. Alves, M. F. Craciun, A. I. S. Neves, *ACS Appl. Mater. Interfaces* **2020**, *12*, 29861.
[69] M. Park, S. J. Hong, K. H. Kim, H. Kang, M. Lee, D. H. Jeong, Y. W. Park, B. H. Kim, *Appl. Phys. Lett.* **2017**, *111*, 173103.
[70] C. H. Park, N. Bonini, T. Sohier, G. Samsonidze, B. Kozinsky, M. Calandra, F. Mauri, N. Marzari, *Nano Lett.* **2014**, *14*, 1113.
[71] D. J. Sánchez-Trujillo, L. V. Osorio-Maldonado, J. J. Prías-Barragán, *Sci. Rep.* **2023**, *13*, 4810.
[72] A. Nag, R. B. V. B. Simorangkir, D. R. Gawade, S. Nuthalapati, J. L. Buckley, B. O'Flynn, M. E. Altinsoy, S. C. Mukhopadhyay, *Mater. Des.* **2022**, *221*, 110971.
[73] S. Zhao, D. Lou, P. Zhan, G. Li, K. Dai, J. Guo, G. Zheng, C. Liu, C. Shen, Z. Guo, *J. Mater. Chem. C* **2017**, *5*, 8233.
[74] Z. Yang, Y. Pang, X. Han, Y. Yang, J. Ling, M. Jian, Y. Zhang, Y. Yang, T. L. Ren, *ACS Nano* **2018**, *12*, 9134.
[75] L. Huang, H. Wang, P. Wu, W. Huang, W. Gao, F. Fang, N. Cai, R. Chen, Z. Zhu, *Sensors* **2020**, *20*, 4266.
[76] Y. Peng, W. Zhao, F. Ni, W. Yu, X. Liu, *ACS Nano* **2021**, *15*, 19490.
[77] F. Yang, C. Yu, J. Liu, Y. Zhang, *presented at 2021 23rd European Microelectronic and Packaging Conf. Exhibition EMPC*, Gothenburg, Sweden, Sep **2021**, 1.
[78] O. Salihoglu, H. B. Uzlu, O. Yakar, S. Aas, O. Balci, N. Kakenov, S. Balci, S. Olcum, S. Süzer, C. Kocabas, *Nano Lett.* **2018**, *18*, 4541.
[79] P. Ding, P. Wang, J. Su, B. Mao, M. Ren, K. Xu, S. Tian, Y. Li, X. Tian, J. Wang, *J. Phys. D: Appl. Phys.* **2022**, *55*, 345103.
[80] S. Huang, N. Wang, J. Bao, H. Ye, D. Zhang, W. Yue, Y. Fu, L. Ye, K. Jeppson, J. Liu, *2016 6th Electronic System-Integration Technology Conference (ESTC)* **2016**, 1.
[81] Z. Chen, K. Yang, T. Xian, C. Kocabas, S. V. Morozov, A. H. Castro Neto, K. S. Novoselov, D. V. Andreeva, M. Koperski, *ACS Appl. Mater. Interfaces* **2021**, *13*, 27278.
[82] D. Ma, X. Li, Y. Guo, Y. Zeng, *IOP Conf. Ser. Earth Environ. Sci.* **2018**, *108*, 022019.
[83] P. Pigeat, D. Rouxel, B. Weber, *Phys. Rev. B: Condens. Matter Mater. Phys.* **1998**, *57*, 9293.
[84] S. T. Mi, Y. C. Zhang, X. Bin Fu, Q. Li, T. Kong, *Optik* **2023**, *290*, 171347.
[85] C. Guo, B. Zhao, S. Fan, *Phys. Rev. X* **2022**, *12*, 21023.
[86] X. M. Sun, D. Y. Cong, Z. Li, Y. L. Zhang, Z. Chen, Y. Ren, K. D. Liss, Z. Y. Ma, R. G. Li, Y. H. Qu, Z. Yang, L. Wang, Y. D. Wang, *Phys. Rev. Mater.* **2019**, *3*, 034404.
[87] C. Kincal, N. Solak, *Nanomaterials* **2024**, *14*, 879.
[88] M. K. Smith, D. X. Luong, T. L. Bougher, K. Kalaitzidou, J. M. Tour, B. A. Cola, *Appl. Phys. Lett.* **2016**, *109*, 253107.
[89] M. Hou, Y. Bu, Y. Chen, Y. Guo, G. Wen, X. Chen, *Int. J. Heat Mass Transf.* **2022**, *197*, 123303.
[90] J. Plante, B. Lee, *NASA Technical Reports Server (NTRS)* **2005**, 20060013394.
[91] M. A. Mccullar, *Thermal Fluids Anal. Workshop (TFAWS 2010)* **2010**.
[92] L. Perrin, F. Cheritel, 41st International Conference on Environmental Systems **2011**, 5027
[93] Y. G. Lv, Y. T. Wang, T. Meng, Q. W. Wang, W. X. Chu, *Energy Storage Sav.* **2024**, *3*, 153.